AGU PUBLICATIONS

Geophysical Research Letters

RESEARCH LETTER
10.1002/2014GL062191

Key Points:
- BC snow albedo forcing in Tibetan Plateau is assessed by a stochastic snow model
- Effects of snow shape and BC-snow mixing as well as BC coating are examined
- BC direct radiative forcing in the Tibetan Plateau is estimated

Correspondence to:
C. He,
cenlinhe@atmos.ucla.edu

Citation:
He, C., Q. Li, K.-N. Liou, Y. Takano, Y. Gu, L. Qi, Y. Mao, and L. R. Leung (2014), Black carbon radiative forcing over the Tibetan Plateau, *Geophys. Res. Lett.*, *41*, doi:10.1002/2014GL062191.

Received 12 OCT 2014
Accepted 2 NOV 2014
Accepted article online 6 NOV 2014

Black carbon radiative forcing over the Tibetan Plateau

Cenlin He[1], Qinbin Li[1], Kuo-Nan Liou[1], Yoshi Takano[1], Yu Gu[1], Ling Qi[1], Yuhao Mao[2], and L. Ruby Leung[3]

[1]Joint Institute for Regional Earth System Science and Engineering and Department of Atmospheric and Oceanic Sciences, University of California, Los Angeles, Los Angeles, California, USA, [2]Institute of Atmospheric Physics, Chinese Academy of Sciences, Beijing, China, [3]Pacific Northwest National Laboratory, Richland, Washington, USA

Abstract We estimate the snow albedo forcing and direct radiative forcing (DRF) of black carbon (BC) in the Tibetan Plateau using a global chemical transport model in conjunction with a stochastic snow model and a radiative transfer model. The annual mean BC snow albedo forcing is 2.9 W m^{-2} averaged over snow-covered plateau regions, which is a factor of 3 larger than the value over global land snowpack. BC-snow internal mixing increases the albedo forcing by 40–60% compared with external mixing, and coated BC increases the forcing by 30–50% compared with uncoated BC aggregates, whereas Koch snowflakes reduce the forcing by 20–40% relative to spherical snow grains. The annual BC DRF at the top of the atmosphere is 2.3 W m^{-2} with uncertainties of −70–85% in the plateau after scaling the modeled BC absorption optical depth to Aerosol Robotic Network observations. The BC forcings are attributed to emissions from different regions.

1. Introduction

Black carbon (BC) is now considered the second most important human emission in terms of its radiative forcing in the present-day atmosphere after carbon dioxide [*Bond et al.*, 2013]. BC heats the atmosphere by absorbing solar radiation (direct radiative forcing (DRF)) [*Jacobson*, 2001], cools the surface by means of atmospheric scattering and absorption [*Ramanathan and Carmichael*, 2008], and reduces snow and ice albedos upon deposition on the surface (snow albedo effect) [*Warren and Wiscombe*, 1985; *Hansen and Nazarenko*, 2004]. Ample evidence have pointed to significant impacts on the rapid retreat of glaciers in the Tibetan Plateau associated with BC deposited in snow [*Xu et al.*, 2009]. The retreat of these glaciers and the associated changes in surface heating may adversely affect freshwater supply and hydrological cycle for much of Asia [*Menon et al.*, 2010]. The snow albedo effect of BC has also been posited as an important driver of the abrupt retreat of Alpine glaciers from the middle nineteenth century [*Painter et al.*, 2013]. Based on observations, *Flanner et al.* [2011] found that the albedo feedback from the Northern Hemisphere cryosphere is substantially stronger than the value estimated from climate models.

Large uncertainties exist in the estimate of both BC DRF and snow albedo forcing over the Tibetan Plateau. Using a chemical transport model (CTM), *Kopacz et al.* [2011] estimated that BC DRF at the top of the atmosphere (TOA) was 0.2–1.7 W m^{-2} at five Tibetan glacial sites and that BC snow albedo forcing was 4–16 W m^{-2} at the same sites. *Wang et al.* [2014], using the same CTM with updates, derived a substantially smaller BC TOA DRF (<0.5 W m^{-2}) across much of the plateau. *Flanner et al.* [2009] estimated an annual BC snow albedo forcing of 1.3 W m^{-2} over the plateau and 10–20 W m^{-2} in spring in parts of the plateau. *Qian et al.* [2011] reported a springtime BC snow albedo forcing of 14–18 W m^{-2} in the western plateau. The preceding studies all assumed external mixing between BC and spherical snow grains. *Flanner et al.* [2012] pointed out that BC-snow internal mixing increases the albedo forcing by 40–80%. *Liou et al.* [2014] illustrated that both BC-snow mixing state and snow grain shape play critical roles in determining snow albedo forcing.

We investigate both BC snow albedo forcing and TOA DRF over the Tibetan Plateau using an extensively evaluated global CTM (Goddard Earth Observing System (GEOS)-Chem) in conjunction with a stochastic snow model and a radiative transfer model (RTM). We systematically examine the effects of BC-snow mixing states (internal versus external mixing), BC coating states (coated versus uncoated), and snow grain shapes (Koch snowflake versus sphere) on snow albedo forcing and its uncertainties. To the best of our knowledge, this is the first attempt to evaluate the effects of multiple inclusions of coated BC in nonspherical

snow grains. Additionally, we quantify the relative contributions to forcing estimates from different BC source regions. Section 2 briefly describes the preceding models and related model simulations. We then discuss BC snow albedo forcing, DRF, and source attributions in section 3. Conclusions are given in section 4.

2. Approach

We employed the GEOS-Chem global 3-D CTM (version 9-01-03, available at http://www.geos-chem.org) to simulate BC distributions. GEOS-Chem is driven by the Goddard Earth Observing System (GEOS-5) meteorological fields with a spatial resolution of 2°×2.5° horizontally and 47 vertical layers and a temporal resolution of 6 h (3 h for surface variables). All model results presented here are for 2006, during which substantial observations over the Tibetan Plateau are available for verification purposes. A detailed description and extensive evaluations of GEOS-Chem simulations of BC in the plateau have been presented by *He et al.* [2014].

We calculated the BC snow albedo forcing using a stochastic snow model [*Liou et al.*, 2014] that explicitly accounts for multiple internal mixing of BC in various types of snow grains. The nonspherical snow grains were constructed in a 3-D coordinate system with multiple BC particles stochastically distributed inside the snow grains. The light absorption and scattering by snow grains and BC were computed by the geometric-optics surface-wave (GOS) approach developed by *Liou et al.* [2010, 2011]. We have extended the original Monte Carlo photon tracing method to snow grains internally mixed with coated BC and assumed that BCs externally mixed in snowpack are in contact with snow grain surfaces rather than in a suspended interstitial state. Thus, this approach accounted for the interaction between snow grains and BC, which differs from the conventional independent scattering assumption for external mixtures, where optical properties are computed separately for BC and snow grains and averaged using respective cross sections as weighting factors [*Warren and Wiscombe*, 1980, 1985]. We have used the conventional independent scattering assumption for external mixture cases only when comparing with previous studies (see Figure 1).

The original surface albedo in the model was from GEOS-5 meteorological fields. For pure snow, the snow albedo was based on observations. The BC-contaminated snow albedo was determined from the adding/doubling method for radiative transfer using 20 homogeneous sublayers with input of the single-scattering properties computed from GOS for various snow grain sizes and shapes and BC mixing conditions. The present snow model does not account for snow aging, a process that may enhance BC snow albedo forcing [*Flanner et al.*, 2012]. In this study, we have assumed a constant snow grain radius of 100 μm (volume-equivalent sphere). Also, for computational expediency, we developed a parametric curve fitting to stochastic snow model results involving snow albedo reduction associated with BC in snow.

The BC concentration in snow was calculated as the ratio of GEOS-Chem-simulated BC deposition flux and GEOS-5 precipitation over the snow-covered regions [*Kopacz et al.*, 2011; *He et al.*, 2014]. The snow cover was prescribed from GEOS-5 meteorological fields. Subsequently, we derived the associated surface radiative forcing by coupling snow albedo reduction with the GEOS-5 incoming solar radiation field following *Wang et al.* [2011].

We applied the Fu-Liou-Gu (FLG) RTM [*Gu et al.*, 2006, 2010] to calculate atmospheric BC DRF. The FLG RTM combines the delta-four-stream approximation for solar flux calculations with the delta-two/four-stream approximation for infrared flux calculations to assure both accuracy and efficiency. Based on absorption band locations, the solar (0–5 μm) and infrared (5–50 μm) spectra are divided into 6 and 12 bands, respectively, within which the correlated *k* distribution method is used to sort gaseous absorption lines. The FLG RTM is not directly coupled with the stochastic snow model such that radiative transfer through the atmosphere and snow are computed separately.

The GEOS-Chem-simulated BC aerosol optical depth (AOD) and GEOS-5 meteorological fields were input to the RTM. We have shown that GEOS-Chem underestimates BC absorption AOD (AAOD) over the Tibetan Plateau and adjacent regions [*He et al.*, 2014]. Such underestimates appear to be common for current global CTMs, which vastly underestimate BC AAOD globally by several folds [*Bond et al.*, 2013]. Following *Bond et al.* [2013], we determined BC DRF by scaling the modeled BC AAOD to Aerosol Robotic Network (AERONET) observations over global continents and reduce the estimated forcing by 15% to account for the incorrect BC vertical distribution. We have reported only instantaneous clear-sky shortwave BC TOA DRF, which is 2 orders of magnitude larger than the corresponding longwave forcing.

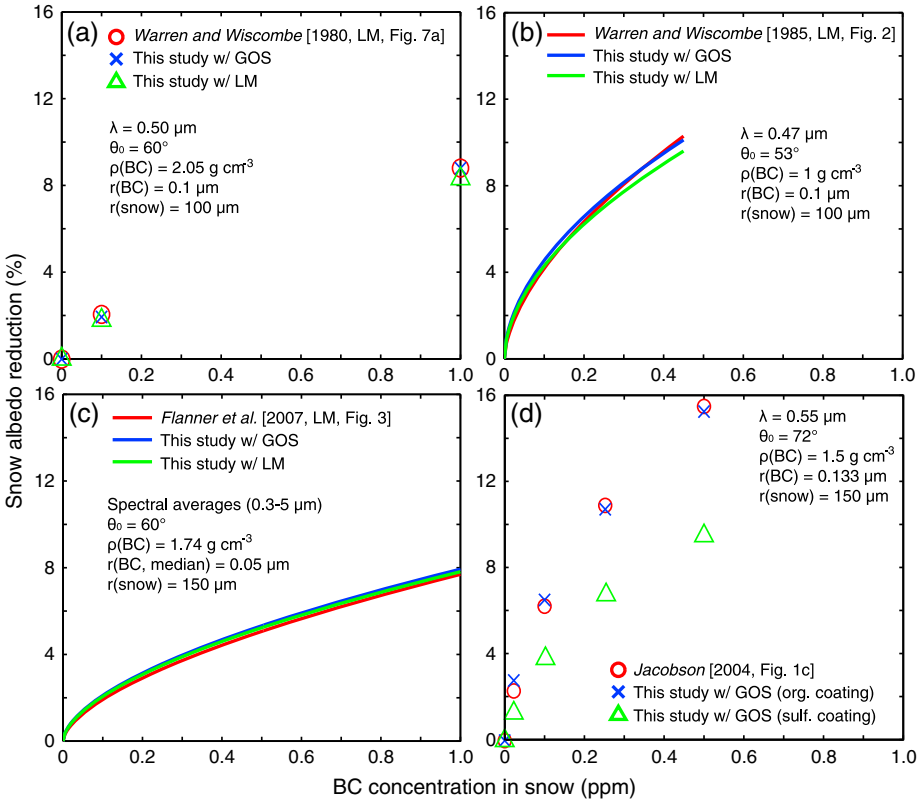

Figure 1. Snow albedo reduction as a function of BC concentration in snow from previous studies (red): (a) *Warren and Wiscombe* [1980], (b) *Warren and Wiscombe* [1985], (c) *Flanner et al.* [2007], and (d) *Jacobson* [2004], compared with this study using the stochastic snow model with the improved geometric-optics surface-wave approach (GOS, blue) and the Lorenz–Mie approach (LM, green) under the same model assumptions, including wavelength (λ), solar zenith angle (θ_0), BC density (ρ), BC, and snow grain radius (r). Results in Figure 1d assume each snow grain including one BC particle and all remaining BCs externally mixed with snow grains. Results from this study in Figure 1d also assume the core-shell structure for BC coated by organics/sulfate with 1 μm diameter [*Schwarz et al.*, 2013].

In addition, we assessed the uncertainty of forcing estimates using a Monte Carlo method [*Efron and Tibshirani*, 1986]. This procedure generates an ensemble of random BC AAODs according to the probability distribution of the GEOS-Chem-simulated BC AAOD (see *He et al.* [2014], Figure 4). Correspondingly, an ensemble of BC DRF is obtained through 5000 valid RTM simulations. The same procedure was repeated for BC snow albedo forcing whereby we randomly varied the BC concentration in snow, snow grain shape, BC-snow mixing state, and BC coating state. We then analyzed the resulting ensemble estimates of the BC forcing statistically, including the mean and confidence interval, and presented the 90% confidence interval as uncertainty range.

3. Results and Discussions

3.1. BC Snow Albedo Forcing

Figure 1 shows the comparison of snow albedo reduction in response to BC in snow between previous modeling studies and the present study under the same model assumptions. This study reproduces (differences of ≤10%) snow albedo reductions from *Warren and Wiscombe* [1980], *Warren and Wiscombe* [1985], and *Flanner et al.* [2007] by using the same Lorenz–Mie (LM) approach, where external mixing of uncoated BC with spherical snow grains was assumed. The resulting small differences are primarily caused by the different methodologies used for solving radiative transfer in snow models. The results computed from the GOS approach are consistent with those computed from the LM theory (Figures 1a–1c). Figure 1d shows a much stronger snow albedo reduction presented by *Jacobson* [2004], who accounted for the internal and external mixing of coated BC with spherical snow grains simultaneously. We have used BC coated by

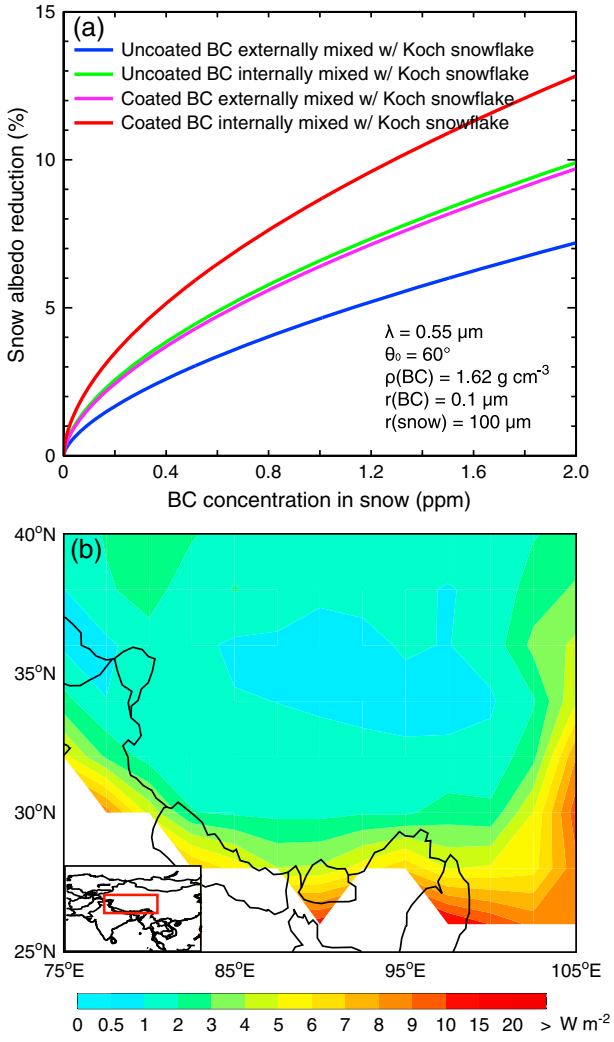

Figure 2. (a) Snow albedo reduction as a function of BC concentration in snow using the stochastic snow model with the improved geometric-optics surface-wave (GOS) approach for internal/external mixing of coated/uncoated BC with Koch snowflakes. Also shown are model parameters including wavelength (λ), solar zenith angle (θ_0), BC density (ρ), BC, and snow grain radius (r). The snow optical depth is set to obtain the observed albedos of pure snow [*Jacobson*, 2004]. The BC density is tuned to obtain a mass absorption coefficient (MAC) of pure BC of 7.5 $m^2\ g^{-1}$. The mass of sulfate coating on BC is tuned to obtain a MAC of coated BC of 11.3 $m^2\ g^{-1}$ [*Bond et al.*, 2006]. (b) Simulated BC snow albedo forcing over the Tibetan Plateau by assuming internal mixing of coated BC with Koch snowflakes. Values are averages for November–April over snow-covered regions.

sulfate and organics in this case, since GEOS-Chem does not simulate the coating of BC by different species dynamically, via condensation and coagulation, in the absence of microphysical processes. Our results, assuming BC coated by sulfate, are 40% lower than those presented in *Jacobson* [2004] but are in good agreement (differences of <8%) with his values (Figure 1d) by assuming organic coating with a refractive index of 1.53–0.02*i* (at 550 nm). We note that the imaginary part (0.02) is at the upper end of the observed values [*Chen and Bond*, 2010]. Moreover, *Ming et al.* [2009], *Yasunari et al.* [2010], and *Hadley et al.* [2010] developed empirical parameterizations of BC-induced snow albedo reductions based on linear regressions of combined results from the abovementioned four modeling studies. However, the snow albedo reductions computed by previous models under assorted assumptions vary by a factor of 2 to 5 (see Figure 1).

Figure 2a shows snow albedo reductions (at 550 nm) as a function of BC concentrations in snow computed from this study by accounting for internal/external mixing of coated/uncoated BC with Koch snowflakes. BC-snow internal mixing enhances snow albedo reduction by 30–90% relative to external mixing, because (1) multiple internal reflections increase the probability of photons being absorbed within snow grains, and (2) the mirror effect enables further absorption enhancement from BC particles that happen to reside near the center of snow grains. Coated BC increases snow albedo reduction by 30–70% relative to uncoated BC aggregates. The use of nonspherical Koch snowflakes leads to 20–40% lower snow albedo reductions than spherical snow grains which produce stronger forward scattering [*Liou et al.*, 2014]. Thus, the use of realistic snow grain shapes could effectively offset the enhancement of snow albedo reduction from BC-snow internal mixing and BC coating. Results presented below were calculated by assuming internal mixing of coated BC with Koch snowflakes.

We calculated the spectrally averaged (0.2–5 μm) (*Liou et al.* [2014]) BC-induced snow albedo reduction in the Tibetan Plateau for 2006. The resulting annual mean reduction is 1.8% over snow-covered regions, with an uncertainty of 1.5–2.0%. The largest reduction is 5% in the southern Himalayas and southeastern plateau, whereas reduction is less than 1% in the central plateau. Observations have shown a mean annual snow

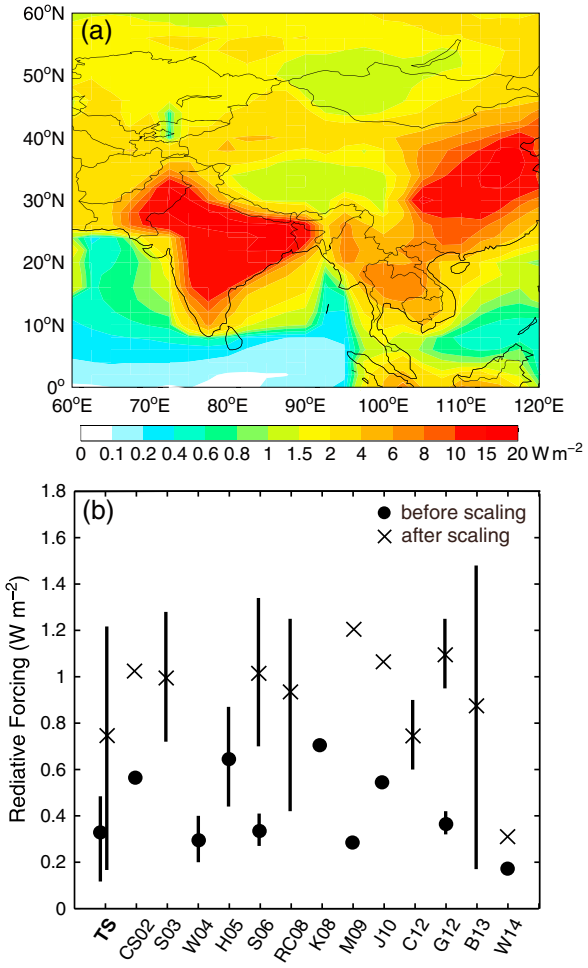

Figure 3. (a) Simulated annual mean BC direct radiative forcing (DRF) at the top of the atmosphere (TOA) over Asia after scaling modeled BC AAOD to AERONET observations. (b) Global annual mean BC TOA DRF before (circle) and after (cross) scaling modeled BC AAOD to AERONET observations: this study (TS), *Chung and Seinfeld* [2002] (CS02), *Sato et al.* [2003] (S03), *Wang* [2004] (W04), *Hansen et al.* [2005] (H05), *Schulz et al.* [2006] (S06), *Ramanathan and Carmichael* [2008] (RC08), *Kim et al.* [2008] (K08), *Myhre et al.* [2009] (M09), *Jacobson* [2010] (J10), *Chung et al.* [2012] (C12), *Ghan et al.* [2012] (G12), *Bond et al.* [2013] (B13), and *Wang et al.* [2014] (W14). Uncertainties (vertical bars) are shown when available.

albedo reduction of 0.4 ± 0.4% during 2000–2009 in the mid-Himalayas [*Ming et al.*, 2012]. That reduction results from the warming produced by many factors such as greenhouse gases and aerosol deposition. Our results show a BC-induced annual snow albedo reduction of 1–2% for 2006 in the same region.

Subsequently, we calculated the BC snow albedo forcing in the Tibetan Plateau averaged for the period November–April (Figure 2b), during which Asian BC emissions are largest [*Lu et al.*, 2012] and snowfall is heaviest [*Pu et al.*, 2007]. The resulting forcing averaged over the region is 2.7 W m^{-2}. The strongest forcing up to 5–10 W m^{-2} is in the southern Himalayas and southeastern plateau (Figure 2b). Our results differ from those of *Qian et al.* [2011], who showed in a modeling analysis that BC snow albedo forcing was higher in the western plateau and much lower in the eastern plateau. The BC snow albedo forcing at five Tibetan glacial sites [cf. *Kopacz et al.*, 2011] is more than fourfold lower in this study than in *Kopacz et al.* [2011]. Seventy percent of the difference is because Kopacz et al. applied *Ming et al.*'s [2009] parameterization that produces considerably larger snow albedo reductions than the present study. Additionally, Kopacz et al. used an earlier version of the GEOS-Chem model that produced higher BC concentrations in snow, which explains about 30% of the difference. *Flanner et al.* [2009] showed an annual mean forcing of 1.3 W m^{-2} over the whole plateau, 30% lower than our corresponding estimate because of the enhancement from BC-snow internal mixing employed in this study. The mean forcing, accounting for different combinations of BC-snow mixing states and BC coating states, is 2.4 W m^{-2} for Koch snowflakes annually over snow-covered Plateau regions, with an uncertainty of 1.5–3.6 W m^{-2}. Furthermore, including various snow grain shapes in the analysis, we estimate an annual mean BC snow albedo forcing of 2.9 W m^{-2}, with an uncertainty of 1.5–5.0 W m^{-2}.

We estimate a global annual mean BC snow albedo forcing of 0.05 W m^{-2}, with an uncertainty of 0.02–0.08 W m^{-2}. The uncertainty range manifests the combined impacts of snow grain shapes, BC-snow mixing states, and BC coating states. Our estimate is in the middle of the range (0.01–0.09 W m^{-2}) presented by *Bond et al.* [2013]. *Flanner et al.* [2007] estimated an annual mean BC snow albedo forcing of 0.55 W m^{-2} averaged over only global land snowpack. Their value is lower than our corresponding estimate (0.86 W m^{-2}) mainly because their model did not account for BC-snow internal mixing, which increases the global BC snow albedo forcing by 40–60% compared with external mixing, within the range of 34–86% reported by *Flanner et al.* [2012].

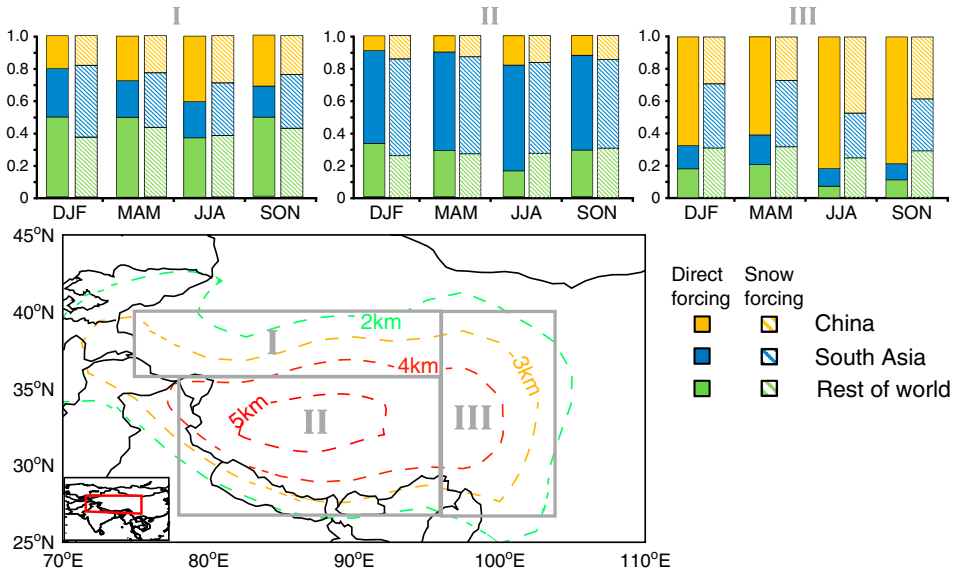

Figure 4. GEOS-Chem-simulated seasonal contributions to BC snow albedo forcing and direct radiative forcing over the Tibetan Plateau (I: the northern plateau, II: the Himalayas and central plateau, and III: the eastern plateau) from BC emissions from China (orange), South Asia (blue), and the rest of the world (green). The results are for 2006. Topography is shown as colored contours.

3.2. BC Direct Radiative Forcing

The annual mean BC TOA DRF before scaling the modeled BC AAOD to AERONET observations is 0.90 W m^{-2} averaged over the plateau, with higher values in spring and summer and lower values in fall and winter. The DRF after the scaling is 2.3 W m^{-2}, with an uncertainty of 0.7–4.3 W m^{-2} without accounting for uncertainty in the AAOD scaling, which is in the range of −60% to 40% [*Bond et al.*, 2013]. The strongest forcing is in the southern Himalayas and to the east of the plateau (Figure 3a). The spatial pattern is consistent with those from *Sato et al.* [2003] and *Chung et al.* [2012], in which AAODs were also similarly scaled. However, the DRF at the five Tibetan glacial sites mentioned above is more than 50% higher in this study than in *Kopacz et al.*'s [2011], who already accounted for BC coating effects. The difference is partially because of lower BC emissions in their study. The surface dimming due to atmospheric BC is −4.7 W m^{-2} annually over the plateau, while the annual mean atmospheric heating rate is larger than 0.2 K d^{-1} near the surface.

The global annual mean BC AAOD after scaling is 0.0041, a factor of 2.5 larger than the modeled values, reflecting the absence of BC internal mixing and low BC emissions in the model. If we attribute the underestimate of modeled AAODs to the weaker BC absorption associated with external mixing, the BC mass absorption coefficient (MAC) in the model needs to be increased from 7 to 14 m^2 g^{-1} to achieve a better agreement with AERONET observations, which is at the upper end of previous estimates (8–14 m^2 g^{-1}) [e.g., *Schulz et al.*, 2006; *Jacobson*, 2010]. Alternatively, a BC MAC of 11.3 m^2 g^{-1} for the mean BC mixing state from atmospheric observations [*Bond et al.*, 2006] requires increasing global BC emissions in the model from 8.1 to 10.4 Tg yr^{-1} to match AERONET observations, which are 40% lower than the global top-down estimation [*Cohen and Wang*, 2014]. The global annual mean TOA DRF is 0.74 W m^{-2} using the scaled AAODs, which are 15% lower than the best estimate from *Bond et al.* [2013]. We also note that the DRF is associated with large uncertainties (Figure 3b) resulting from factors including BC mixing state and emissions used in models. Our best estimate is more than a factor of 2 higher than that from *Wang et al.* [2014], primarily because of lower BC emissions and smaller absorption forcing efficiency (AFE), (ratio of DRF to AAOD [*Schulz et al.*, 2006]) used in their study. Our global annual mean AFE (180 W m^{-2} $AAOD^{-1}$) is larger than previous estimates (97–177 W m^{-2} $AAOD^{-1}$) [e.g., *Jacobson*, 2010; *Chung et al.*, 2012], a direct result of the large BC loading at altitudes above 5 km in our model. This is likely a result of an overlong BC lifetime due to insufficient scavenging in the model. *Wang et al.* [2014] suggested that BC wet scavenging in GEOS-Chem is too weak based on comparisons with aircraft measurements over the Pacific Ocean.

3.3. Source Attribution to BC Forcings

Figure 4 shows the contributions of BC emissions from China, South Asia (including India and Southeast Asia) and the rest of the world to BC snow albedo forcing and TOA DRF over the plateau. The northern plateau (region I, Figure 4) is mainly influenced by the northern midlatitude BC pollution transported by the westerlies [*Kopacz et al.*, 2011; *Lu et al.*, 2012], which accounts for half of both snow albedo forcing and DRF in the region. The anthropogenic BC emissions from South Asia (90% of its total BC emissions) dominate both BC snow albedo forcing and DRF in the central plateau and the Himalayas (region II, Figure 4), reflecting the regions' proximity to large sources in India [*Lu et al.*, 2012]. In the eastern plateau (region III, Figure 4), anthropogenic BC emissions from China (>90% of its total BC emissions) dominate the contribution to BC DRF throughout the year (70%), which is in line with the results presented by *Kopacz et al.* [2011]. However, China accounts for less than half of the snow albedo forcing in the eastern Plateau, comparable to the contribution from South Asia. This is because the fraction (70%) of hydrophilic BC upon arriving in the eastern plateau after having been emitted from China is smaller than the fraction (90%) upon reaching the region after having been emitted from South Asia, which reflects the proximity of the eastern plateau to large BC sources in Southwest China, leading to less efficient wet scavenging and hence lower BC concentrations in snow.

4. Conclusions

We have estimated both BC snow albedo forcing and TOA DRF over the Tibetan Plateau using a systematically evaluated global CTM in conjunction with a stochastic snow model and a RTM. The annual mean BC snow albedo forcing in snow-covered plateau regions, accounting for various snow grain shapes, BC-snow mixing states, and BC coating states, is 1.5–5.0 W m^{-2}. A robust estimate of BC snow albedo forcing in the plateau is very difficult in view of the scarcity of measurements of BC concentrations in snow that vary spatiotemporally across the plateau and large uncertainties associated with BC-induced snow albedo reduction. The estimated snow albedo reductions differ by up to a factor of 4 depending on snow grain shape, BC-snow mixing state, and BC coating state. Further investigations of the important snow aging processes, including wind pumping and sintering, are necessary to understand the albedo forcing [*Flanner et al.*, 2012]. The combined effects produced by snow grain shape, BC-snow mixing, BC coating, and snow aging should be simultaneously taken into account to make further advances to reduce uncertainties in BC snow albedo forcing estimates. Additionally, our best estimate of the annual mean BC TOA DRF is 2.3 W m^{-2} in the plateau with uncertainties of −75–85%, which stem primarily from uncertainties associated with modeled BC AAOD. This calls for concerted measurements of BC vertical profiles, particularly in mountainous regions such as the Tibetan Plateau.

Acknowledgments

This study was funded by NASA grants NNX09AF07G and NNX08AF64G from the Atmospheric Chemistry Modeling and Analysis Program and by DOE grant DESC0006742. We thank J. Zhang and M. Gao for their help in this work. Users can access the data from this paper via the authors without any restrictions.

The Editor thanks two anonymous reviewers for their assistance in evaluating this paper.

References

Bond, T. C., G. Habib, and R. W. Bergstrom (2006), Limitations in the enhancement of visible light absorption due to mixing state, *J. Geophys. Res.*, *111*, D20211, doi:10.1029/2006JD007315.

Bond, T. C., et al. (2013), Bounding the role of black carbon in the climate system: A scientific assessment, *J. Geophys. Res. Atmos.*, *118*, 5380–5552, doi:10.1002/jgrd.50171.

Chen, Y., and T. C. Bond (2010), Light absorption by organic carbon from wood combustion, *Atmos. Chem. Phys.*, *10*(4), 1773–1787, doi:10.5194/acp-10-1773-2010.

Chung, C. E., V. Ramanathan, and D. Decremer (2012), Observationally constrained estimates of carbonaceous aerosol radiative forcing, *Proc. Natl. Acad. Sci. U.S.A.*, *109*(29), 11,624–11,629, doi:10.1073/pnas.1203707109.

Chung, S. H., and J. H. Seinfeld (2002), Global distribution and climate forcing of carbonaceous aerosols, *J. Geophys. Res.*, *107*(D19), 4407, doi:10.1029/2001JD001397.

Cohen, J. B., and C. Wang (2014), Estimating global black carbon emissions using a top-down Kalman Filter approach, *J. Geophys. Res. Atmos.*, *119*, 307–323, doi:10.1002/2013JD019912.

Efron, B., and R. Tibshirani (1986), Bootstrap methods for standard errors, confidence intervals, and other measures of statistical accuracy, *Stat. Sci.*, *1*(1), 54–75.

Flanner, M. G., C. S. Zender, J. T. Randerson, and P. J. Rasch (2007), Present-day climate forcing and response from black carbon in snow, *J. Geophys. Res.*, *112*, D11202, doi:10.1029/2006JD008003.

Flanner, M. G., C. S. Zender, P. G. Hess, N. M. Mahowald, T. H. Painter, V. Ramanathan, and P. J. Rasch (2009), Springtime warming and reduced snow cover from carbonaceous particles, *Atmos. Chem. Phys.*, *9*(7), 2481–2497, doi:10.5194/acp-9-2481-2009.

Flanner, M. G., K. M. Shell, M. Barlage, D. K. Perovich, and M. A. Tschudi (2011), Radiative forcing and albedo feedback from the Northern Hemisphere cryosphere between 1979 and 2008, *Nat. Geosci.*, *4*(3), 151–155, doi:10.1038/Ngeo1062.

Flanner, M. G., X. Liu, C. Zhou, J. E. Penner, and C. Jiao (2012), Enhanced solar energy absorption by internally-mixed black carbon in snow grains, *Atmos. Chem. Phys.*, *12*(10), 4699–4721, doi:10.5194/acp-12-4699-2012.

Ghan, S. J., X. Liu, R. C. Easter, R. Zaveri, P. J. Rasch, J.-H. Yoon, and B. Eaton (2012), Toward a Minimal Representation of Aerosols in Climate Models: Comparative Decomposition of Aerosol Direct, Semidirect, and Indirect Radiative Forcing, *J. Clim.*, *25*(19), 6461–6476, doi:10.1175/Jcli-D-11-00650.1.

Gu, Y., K. N. Liou, Y. Xue, C. R. Mechoso, W. Li, and Y. Luo (2006), Climatic effects of different aerosol types in China simulated by the UCLA general circulation model, *J. Geophys. Res.*, *111*, D15201, doi:10.1029/2005JD006312.
Gu, Y., K. N. Liou, W. Chen, and H. Liao (2010), Direct climate effect of black carbon in China and its impact on dust storms, *J. Geophys. Res.*, *115*, D00K14, doi:10.1029/2009JD013427.
Hadley, O. L., C. E. Corrigan, T. W. Kirchstetter, S. S. Cliff, and V. Ramanathan (2010), Measured black carbon deposition on the Sierra Nevada snow pack and implication for snow pack retreat, *Atmos. Chem. Phys.*, *10*(15), 7505–7513, doi:10.5194/acp-10-7505-2010.
Hansen, J., and L. Nazarenko (2004), Soot climate forcing via snow and ice albedos, *Proc. Natl. Acad. Sci. U.S.A.*, *101*(2), 423–428, doi:10.1073/pnas.2237157100.
Hansen, J., et al. (2005), Efficacy of climate forcings, *J. Geophys. Res.*, *110*, D18104, doi:10.1029/2005JD005776.
He, C., et al. (2014), A global 3-D CTM evaluation of black carbon in the Tibetan Plateau, *Atmos. Chem. Phys.*, *14*, 7091–7112, doi:10.5194/acp-14-7091-2014.
Jacobson, M. Z. (2001), Strong radiative heating due to the mixing state of black carbon in atmospheric aerosols, *Nature*, *409*(6821), 695–697, doi:10.1038/35055518.
Jacobson, M. Z. (2004), Climate response of fossil fuel and biofuel soot, accounting for soot's feedback to snow and sea ice albedo and emissivity, *J. Geophys. Res.*, *109*, D21201, doi:10.1029/2004JD004945.
Jacobson, M. Z. (2010), Short-term effects of controlling fossil-fuel soot, biofuel soot and gases, and methane on climate, Arctic ice, and air pollution health, *J. Geophys. Res.*, *115*, D14209, doi:10.1029/2009JD013795.
Kim, D., C. Wang, A. M. L. Ekman, M. C. Barth, and P. J. Rasch (2008), Distribution and direct radiative forcing of carbonaceous and sulfate aerosols in an interactive size-resolving aerosol-climate model, *J. Geophys. Res.*, *113*, D16309, doi:10.1029/2007JD009756.
Kopacz, M., D. L. Mauzerall, J. Wang, E. M. Leibensperger, D. K. Henze, and K. Singh (2011), Origin and radiative forcing of black carbon transported to the Himalayas and Tibetan Plateau, *Atmos. Chem. Phys.*, *11*(6), 2837–-2852, doi:10.5194/acp-11-2837-2011.
Liou, K. N., Y. Takano, and P. Yang (2010), On geometric optics and surface waves for light scattering by spheres, *J. Quant. Spectrosc. Radiat. Transfer*, *111*, 1980–1989, doi:10.1016/j.jqsrt.2010.04.004.
Liou, K. N., Y. Takano, and P. Yang (2011), Light absorption and scattering by aggregates: Application to black carbon and snow grains, *J. Quant. Spectrosc. Radiat. Transfer*, *112*(10), 1581–1594, doi:10.1016/j.jqsrt.2011.03.007.
Liou, K. N., Y. Takano, C. He, P. Yang, L. R. Leung, Y. Gu, and W. L. Lee (2014), Stochastic parameterization for light absorption by internally mixed BC/dust in snow grains for application to climate models, *J. Geophys. Res. Atmos.*, *119*, 7616–7632, doi:10.1002/2014JD021665.
Lu, Z. F., D. G. Streets, Q. Zhang, and S. W. Wang (2012), A novel back trajectory analysis of the origin of black carbon transported to the Himalayas and Tibetan Plateau during 1996-2010, *Geophys. Res. Lett.*, *39*, L01809, doi:10.1029/2011GL049903.
Menon, S., D. Koch, G. Beig, S. Sahu, J. Fasullo, and D. Orlikowski (2010), Black carbon aerosols and the third polar ice cap, *Atmos. Chem. Phys.*, *10*(10), 4559–4571, doi:10.5194/acp-10-4559-2010.
Ming, J., C. D. Xiao, H. Cachier, D. Qin, X. Qin, Z. Li, and J. Pu (2009), Black Carbon (BC) in the snow of glaciers in west China and its potential effects on albedos, *Atmos. Res.*, *92*(1), 114–123, doi:10.1016/j.atmosres.2008.09.007.
Ming, J., Z. C. Du, C. D. Xiao, X. Xu, and D. Zhang (2012), Darkening of the mid-Himalaya glaciers since 2000 and the potential causes, *Environ. Res. Lett.*, *7*(1), 014021, doi:10.1088/1748-9326/7/1/014021.
Myhre, G., et al. (2009), Modelled radiative forcing of the direct aerosol effect with multi-observation evaluation, *Atmos. Chem. Phys.*, *9*(4), 1365–1392, doi:10.5194/acp-9-1365-2009.
Painter, T. H., M. G. Flanner, G. Kaser, B. Marzeion, R. A. VanCuren, and W. Abdalati (2013), End of the Little Ice Age in the Alps forced by industrial black carbon, *Proc. Natl. Acad. Sci. U.S.A.*, *110*(38), 15,216–15,221, doi:10.1073/pnas.1302570110.
Pu, Z., L. Xu, and V. V. Salomonson (2007), MODIS/Terra observed seasonal variations of snow cover over the Tibetan Plateau, *Geophys. Res. Lett.*, *34*, L06706, doi:10.1029/2007GL029262.
Qian, Y., M. G. Flanner, L. R. Leung, and W. Wang (2011), Sensitivity studies on the impacts of Tibetan Plateau snowpack pollution on the Asian hydrological cycle and monsoon climate, *Atmos. Chem. Phys.*, *11*(5), 1929–1948, doi:10.5194/acp-11-1929-2011.
Ramanathan, V., and G. Carmichael (2008), Global and regional climate changes due to black carbon, *Nat. Geosci.*, *1*(4), 221–227, doi:10.1038/Ngeo156.
Sato, M., J. Hansen, D. Koch, A. Lacis, R. Ruedy, O. Dubovik, B. Holben, M. Chin, and T. Novakov (2003), Global atmospheric black carbon inferred from AERONET, *Proc. Natl. Acad. Sci. U.S.A.*, *100*(11), 6319–6324, doi:10.1073/pnas.0731897100.
Schulz, M., et al. (2006), Radiative forcing by aerosols as derived from the AeroCom present-day and pre-industrial simulations, *Atmos. Chem. Phys.*, *6*, 5225–5246.
Schwarz, J. P., R. S. Gao, A. E. Perring, J. R. Spackman, and D. W. Fahey (2013), Black carbon aerosol size in snow, *Sci. Rep. UK*, *3*, 1356, doi:10.1038/srep01356.
Wang, C. (2004), A modeling study on the climate impacts of black carbon aerosols, *J. Geophys. Res.*, *109*, D03106, doi:10.1029/2003JD004084.
Wang, Q., et al. (2011), Sources of carbonaceous aerosols and deposited black carbon in the Arctic in winter-spring: Implications for radiative forcing, *Atmos. Chem. Phys.*, *11*(23), 12,453–12,473, doi:10.5194/acp-11-12453-2011.
Wang, Q. Q., D. J. Jacob, J. R. Spackman, A. E. Perring, J. P. Schwarz, N. Moteki, E. A. Marais, C. Ge, J. Wang, and S. R. H. Barret (2014), Global budget and radiative forcing of black carbon aerosol: Constraints from pole-to-pole (HIPPO) observations across the Pacific, *J. Geophys. Res. Atmos.*, *119*, 195–206, doi:10.1002/2013JD020824.
Warren, S. G., and W. J. Wiscombe (1980), A Model for the Spectral Albedo of Snow. 2. Snow Containing Atmospheric Aerosols, *J. Atmos. Sci.*, *37*(12), 2734–2745.
Warren, S. G., and W. J. Wiscombe (1985), Dirty Snow after Nuclear-War, *Nature*, *313*(6002), 467–470, doi:10.1038/313467a0.
Xu, B. Q., et al. (2009), Black soot and the survival of Tibetan glaciers, *Proc. Natl. Acad. Sci. U.S.A.*, *106*(52), 22,114–22,118, doi:10.1073/pnas.0910444106.
Yasunari, T. J., P. Bonasoni, P. Laj, K. Fujita, E. Vuillermoz, A. Marinoni, P. Cristofanelli, R. Duchi, G. Tartari, and K.-M. Lau (2010), Estimated impact of black carbon deposition during pre-monsoon season from Nepal Climate Observatory - Pyramid data and snow albedo changes over Himalayan glaciers, *Atmos. Chem. Phys.*, *10*(14), 6603–6615, doi:10.5194/acp-10-6603-2010.